

RESEARCH

Open Access



Study on Preparation and Thermophysical Properties of Binary Paraffin Phase Change Concrete

Zhiwen Jia^{1*} , Dongwei Li^{2*}, Zecheng Wang¹, Zhenhua Wang¹ and Fang Fang¹

Abstract

The binary phase change paraffin (BP) was prepared using the melt blending method, followed by adsorption and encapsulation to produce the phase change aggregate. Phase change concrete was subsequently prepared using the volumetric replacement method. The study examined the thermal properties of BP, along with the semi-adiabatic temperature rise and thermal conductivity of the phase change concrete at different replacement rates. The results indicate that BP exhibits two plateau regions, with phase change intervals varying according to the mass ratio. The high-temperature phase change interval ranges from 18.3 °C to 47.3 °C, while the low-temperature phase change interval ranges from 0.1 °C to 4.6 °C. When the mass ratio of 48# paraffin to 5# paraffin is 7:3, the peak phase change temperatures are 2.58 °C and 44.52 °C, with corresponding enthalpies of 66.52 J/g and 102.63 J/g, respectively. The addition of phase change aggregate effectively reduces the hydration temperature rise of concrete, slows the rate of temperature increase, and decreases the thermal conductivity. The semi-adiabatic temperature rise curve of the phase change concrete exhibits an "S"-shaped variation over time, with the composite exponential function providing a more accurate representation of this process.

Keywords Binary phase change paraffin, Phase change concrete, Semi-adiabatic temperature rise, Thermal properties

1 Introduction

Owing to its exceptional mechanical properties, durability, and construction efficiency, mass concrete demonstrates significant potential across diverse engineering domains, including large reservoir dams (Afzal et al., 2022; Singh et al., 2024), bridges (Wang et al., 2020), tunnels (Li et al., 2023), deep shafts (Zhang et al., 2016, 2022;

Zhou et al., 2017), and foundations (Smolana et al., 2021). Following the pouring of concrete, the swift progression of the hydration reaction induces a marked temperature increase (Xie et al., 2023; Zhang et al., 2023). Concurrently, the low thermal conductivity of concrete hinders the rapid dissipation of internal heat, while the surface undergoes rapid cooling due to environmental influences (Mardmomen & Chen, 2023). The thermal stress arising from this temperature differential is the primary factor leading to the cracking of concrete structures (Li et al., 2022; Wang et al., 2023; Zhang, 2023), thereby posing substantial risks to construction safety and the long-term stability of the structure.

To mitigate the risk of cracking in mass concrete resulting from thermal stress, the implementation of effective temperature control measures is of paramount importance. These strategies encompass the optimization of

Journal information: ISSN 1976-0485 / eISSN 2234-1315.

*Correspondence:

Zhiwen Jia

zwjia518@163.com

Dongwei Li

lidongwei@dlu.edu.cn

¹ School of Civil and Architectural Engineering, East China University of Technology, Nanchang 330013, China

² College of Civil Engineering and Architecture, Dalian University, Dalian 116622, China



© The Author(s) 2024. **Open Access** This article is licensed under a Creative Commons Attribution 4.0 International License, which permits use, sharing, adaptation, distribution and reproduction in any medium or format, as long as you give appropriate credit to the original author(s) and the source, provide a link to the Creative Commons licence, and indicate if changes were made. The images or other third party material in this article are included in the article's Creative Commons licence, unless indicated otherwise in a credit line to the material. If material is not included in the article's Creative Commons licence and your intended use is not permitted by statutory regulation or exceeds the permitted use, you will need to obtain permission directly from the copyright holder. To view a copy of this licence, visit <http://creativecommons.org/licenses/by/4.0/>.

the concrete mix design, the precooling of raw materials, and the regulation of curing temperature, all aimed at minimizing peak temperatures and temperature differentials. Specifically, the partial substitution of ordinary cement clinker with mineral admixtures and low-heat Portland cement can markedly diminish the heat released during the hydration process (Hamid & Chorzepa, 2020; Luo et al., 2023; Wang et al., 2022). Additionally, the precooling of aggregates and mixing water, for instance, through the incorporation of ice chips or the application of air-cooling techniques, represents an effective method of temperature control (Li et al., 2020; Shen et al., 2022). The embedding of cold water pipes coupled with the utilization of a circulating water cooling system further enhances the control of temperature rise within the concrete, thereby mitigating the risk of crack formation (Lu et al., 2021; Tasri & Susilawati, 2019; Tran et al., 2023). Nevertheless, while these cooling methods are effective in mitigating internal temperature rises, they may concurrently exert adverse effects on the overall performance of the concrete structure (Zhao et al., 2019). Improper application of these techniques may, in fact, exacerbate the cracking issues within concrete structures (Wang et al., 2022).

Phase Change Materials (PCMs) possess the ability to absorb or release substantial amounts of heat during phase transitions, all while maintaining a constant temperature. Presently, organic phase change materials have found extensive application in the construction sector, attributed to their high latent heat and excellent thermal stability (Berardi & Gallardo, 2019). However, the fixed phase transition temperatures of existing phase change materials may not entirely fulfill the diverse requirements of construction projects. To surmount this limitation, researchers have successfully developed composite phase change materials with enhanced applicability by blending two or more phase change materials (Bai et al., 2022; Chen Chang et al. 2022). By adjusting the blending ratios of these materials, phase change materials with tailored phase transition temperatures can be produced, better accommodating the specific requirements of various construction projects (Ghadim et al., 2019). The development of composite phase change materials not only broadens the applicability of these materials but also facilitates their use in phase change concrete, particularly in the realms of building energy efficiency (Lv et al., 2017; Shu Zhao et al. 2021) and the freeze–thaw resistance of concrete structures in cold regions (Dong et al., 2024; Tian et al., 2022).

The integration of phase change materials (PCMs) into mass concrete is intended to harness their capacity to absorb or release substantial amounts of heat during phase transitions, thereby facilitating the effective

regulation of temperature rise during the hydration process and preventing the formation of thermal cracks. Researchers have identified the optimal phase transition temperature range of PCMs in mass concrete through extensive studies (Fernandes et al., 2014) and, leveraging these insights, have developed and formulated corresponding PCMs that have been successfully implemented in mass concrete (Kim et al., 2015; Li et al., 2024; Mandal et al., 2022). Findings from the (semi-)adiabatic temperature rise tests reveal that this application significantly mitigates the maximum temperature rise during the hydration process and effectively decelerates the rate of temperature increase (Ju et al., 2023; Kheradmand et al., 2019; Yun et al., 2019). Furthermore, by simulating the influence of key PCM parameters under (semi-)adiabatic conditions on temperature evolution and tensile stress development, researchers have further substantiated the pronounced efficacy of PCMs in mitigating thermal stress and preventing cracks induced by temperature gradients (Savija & Schlangen, 2016). Although the application of phase change concrete in hydration heat control has achieved notable progress, research on the pronounced cooling effects of environmental temperature on the external surface of concrete remains relatively scarce. Additionally, current research on the adiabatic temperature rise models of phase change concrete remains limited, thereby constraining a comprehensive understanding of the thermal behavior of phase change concrete.

In this study, a binary phase change paraffin system was prepared via the melt blending method, and the behavior of phase transformation storage and heat release was systematically analyzed using non-cooling curve tests, differential scanning calorimetry (DSC) tests, cooling and heating curve tests, and phase change cycling tests. Expanded perlite was employed as the carrier material, while cement paste served as the encapsulation material, to fabricate phase change fine aggregate, whose stability was subsequently evaluated. The phase change fine aggregate was incorporated into the concrete using the volumetric replacement method. The effects of aggregate replacement rate on the semi-adiabatic temperature rise and thermal conductivity of the concrete were systematically investigated. This research aims to develop a binary phase change material capable of both controlling hydration heat and mitigating the impact of external environmental factors on concrete. Additionally, the study proposes a semi-adiabatic temperature rise model for phase change concrete that considers the effects of aggregate replacement rate, ultimately enhancing the application of composite phase change materials in mass concrete structures in cold regions.

2 Experiment

2.1 Materials

The phase change materials employed consist of 48# block fully refined paraffin (48#P) and 5# liquid phase change wax (5#P), with phase transition temperatures of 50 °C and 5 °C, respectively, and latent heat values of 136.78 J/g and 200.84 J/g. The carrier material selected is expanded perlite, with its fundamental properties outlined in Table 1. Portland cement used is P.O 42.5R ordinary Portland cement. Fly ash is classified as class I fly ash, with a density of 2.55 g cm⁻³. Silica powder is 98-grade silica powder, with a SiO₂ content of 98.4. The water-reducing agent employed is a polycarboxylate high-efficiency water reducer, with a water-reducing rate greater than 15%. Coarse aggregate comprises continuously graded natural crushed stone with particle sizes ranging from 5 to 20 mm. Fine aggregate consists of river sand, with a fineness modulus of 2.48.

2.2 Preparation

2.2.1 Preparation of BP

BP was prepared utilizing the melt blending method, as shown in Fig. 1. Specific quantities of melted 5#P and 48#P (mass ratio = 1:9, 2:8, 3:7, 4:6, 5:5, 6:4, 7:3, 8:2, 9:1) were measured and combined in the same beaker. The mixture was placed in a constant temperature magnetic stirrer (60 °C) and stirred continuously for 60 min to ensure thorough blending of the two paraffins. Each proportioned solution was assigned a numerical code, with

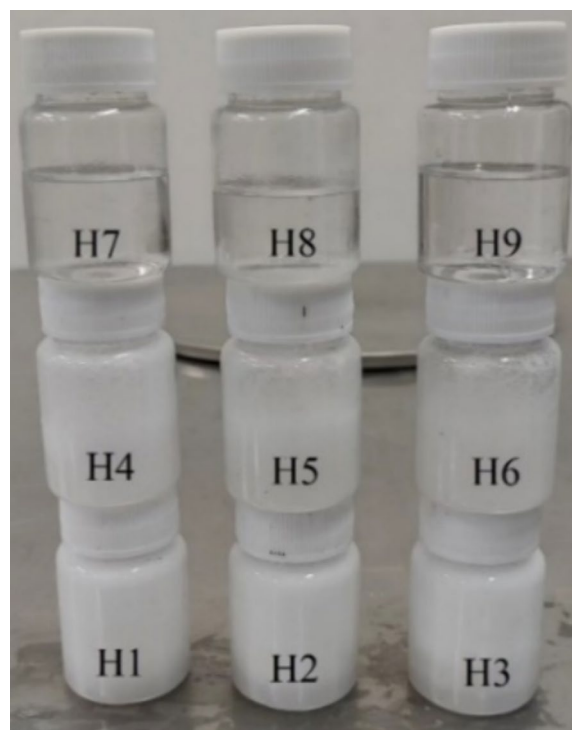


Fig. 2 Binary melting phase change paraffin

H1 through H9 corresponding to the mass ratios from 1:9 to 9:1, respectively. As illustrated in Fig. 2, at room temperature (27 °C), H1, H2, and H3 exist in a solid state, H4, H5, and H6 exhibit a gel-like state, while H7, H8, and H9 are in a liquid state.

Table 1 Basic properties of EP

Particle size (mm)	Thermal conductivity [W/(m k)]	Bulk density (g cm ⁻³)	Apparent density (g cm ⁻³)	Cylinder compressive strength (kPa)	Water absorption in 1 h (%)
1.18–4.75	0.025–0.049	160.6	408.3	0.418	74.3%

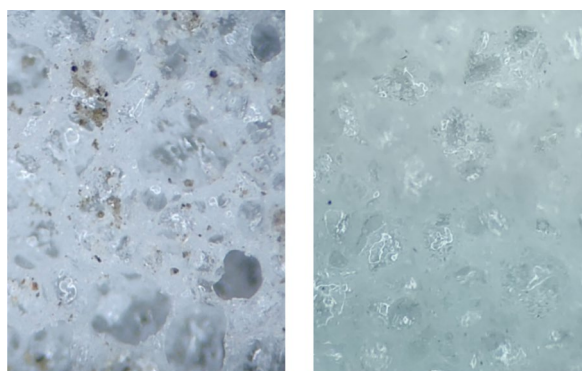
2.2.2 Preparation of Phase Change Aggregate

Preparation of Phase Change Aggregates Involves Adsorption Followed by Encapsulation:

Adsorption: Dried expanded perlite (EP) was immersed in a phase change solution for 12 h to ensure thorough adsorption of the phase change material. Afterward, the



Fig. 1 The preparation flowchart of BP



(a) Before adsorption
Fig. 3 Microscopic image of EP

EP was retrieved, and excess surface solution was filtered off. The material was then cooled, forming the phase change aggregate designated as EP_A, with an apparent density of 0.850 g cm⁻³.

Encapsulation: EP_A was encapsulated using cement through both dry and wet methods.

- (1) Dry Encapsulation: EP_A was soaked in water for 5 min and then removed. Cement powder and EPA were mixed in a 1:1 ratio for 90 s. The mixture was then passed through a vibrating sieve for 90 s to remove excess cement powder, producing the dry-

- encapsulated phase change aggregate, designated as EP_{AD}, with an apparent density of 1.182 g cm⁻³.
- (2) Wet Encapsulation: A water-to-cement ratio of 0.5 was used to prepare the cement paste, which was mixed for 90 s. EP_A with an equal mass to the cement, was then added and mixed for an additional 90 s to ensure even distribution. The mixture was poured onto a 1 mm sieve, vibrated for 90 s, and air-dried to solidify, resulting in the wet-encapsulated phase change aggregate, designated as EP_{AW}, with an apparent density of 1.036 g cm⁻³.

Figure 3 depicts the magnified cross-section of EP before and after adsorption under a microscope at 20× magnification. EP exhibits a well-developed honeycomb-like structure internally, forming interconnected pore channels conducive to storing phase change materials. Following a 12-h adsorption period, nearly all of the internal pores of EP are filled with the phase change material, giving the cross-section the appearance of a film under the microscope.

2.2.3 Preparation of Phase Change Concrete

Mix design was conducted in accordance with the “Code for Mix Design of Ordinary Concrete” (JDJ 55-2011). Phase change concrete was prepared by substituting fine

Table 2 The mix ratio of concrete

Serial number	Cement	Fly ash	Silica powder	Water-reducing agent	Coarse aggregate	Water	Fine aggregate	Phase change aggregate
R-0	385.0	110.0	55.0	5.5	1089.3	192.5	612.7	0
R-1	385.0	110.0	55.0	5.5	1089.3	192.5	551.43	22.75
R-2	385.0	110.0	55.0	5.5	1089.3	192.5	490.16	45.50
R-3	385.0	110.0	55.0	5.5	1089.3	192.5	428.89	68.25
R-4	385.0	110.0	55.0	5.5	1089.3	192.5	367.62	91.00
R-5	385.0	110.0	55.0	5.5	1089.3	192.5	306.35	113.76

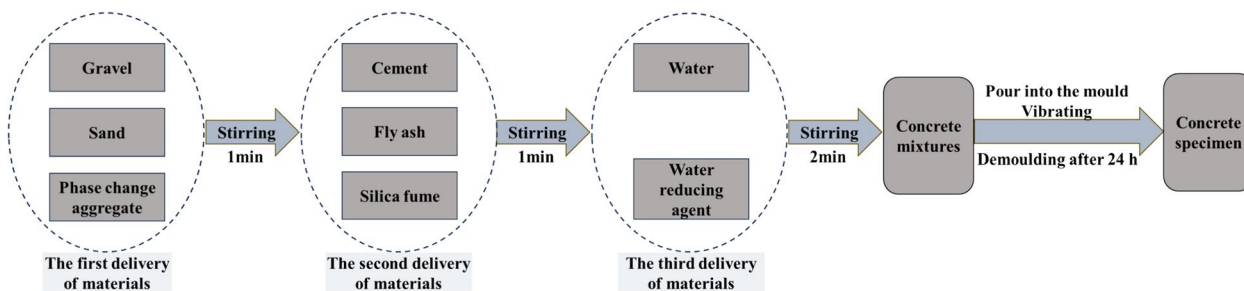


Fig. 4 Flowchart of phase change concrete preparation

aggregates with phase change aggregates at equal volume. The specific mix proportions are detailed in Table 2, while the concrete preparation process is illustrated in Fig. 4.

2.3 Testing Method

2.3.1 Hot Melt-Step Cooling Test

The test tube containing binary paraffin was put into a 55 °C constant temperature water bath, and inserted a thermocouple in the center of the test tube after the BP are completely melted and ensure that it does not touch the inner wall of the tube. Meantime, heat it in a 55 °C of water bath for 1 h. Then, the sample was quickly placed into a - 14 °C low temperature water bath until a complete crystallization is achieved. Finally, the sample was quickly placed into a 55 °C constant temperature water bath until completely melted. The thermal couple was connected to a temperature inspection instrument and the sample temperature was recorded continuously with an interval of 1 min.

2.3.2 Sample Characterization

The phase transition temperature and latent heat of binary paraffin were measured by DSC (NETZSCH DSC214) the test conditions of which are the sample mass of 5–7 mg, the temperature range of - 30 °C to 70 °C, temperature rise and fall rate of 5 °C/min, N₂ atmosphere and nitrogen flow 50 mL/min. To explore the thermal stability of BP, the prepared sample is put into a high and low temperature circulation box, the temperature is set at 55 °C for 1 h to completely melt the sample, and then the sample is completely crystallized by cooling to - 14 °C for 4 h, and finally heated to 55 °C for 1 h the above experimental process was cycled for 50, 100, and 200 times. The step cooling test was carried out when the number of cycles reached 0, 50, 100, and 200 cycles.

2.3.3 Encapsulation Effectiveness Test of Phase Change Aggregates

To evaluate the encapsulation effectiveness of the phase change aggregates, the prepared samples were placed in an oven set to 90 °C, with mass changes recorded after 12, 24, 36, and 48 h. Additionally, these samples were subjected to high and low temperature cycling, with mass changes noted after 5, 10, 20, 50, 100, and 200 cycles.

2.3.4 Thermal Conductivity Test of Phase Change Concrete

The TC3000E transient hot wire thermal conductivity meter was used to measure the thermal conductivity.

The specimens, cubic blocks measuring 100 mm by 100 mm by 100 mm, were air-dried for 24 h before testing. During testing, the probe was placed between two samples, with a test voltage of 1.5 V and a test temperature of 25 °C.

2.3.5 Semi-adiabatic Temperature Rise Test of Phase Change Concrete

The semi-adiabatic chamber comprises two components: a foam mold with internal dimensions of 160 mm by 160 mm by 120 mm, and a wall thickness of 15 mm, and a polystyrene foam board insulation layer (density $\geq 15 \text{ g cm}^{-3}$) with external dimensions of 600 mm by 600 mm by 500 mm, simulating an adiabatic environment. The detailed experimental procedures are outlined as follows:

- (1) Assembly of the semi-adiabatic chamber: The insulation layer is assembled from three polystyrene foam board joined together. Each layer is sealed and bonded with double-sided adhesive. A cuboid region measuring 190mm by 190mm by 160mm is cut out from the middle section of the intermediate foam board layer, where the foam mold is embedded. A 20 mm thick compressible insulation cotton layer is inserted between the intermediate and upper layer. Additionally, an 80kg weight is placed on top of the chamber to enhance its insulation effectiveness. The specific model is illustrated in Fig. 5.
- (2) Concrete pouring: The mixture is poured into the insulation foam mold in two batches, then compacted, with temperature sensors positioned at the center of the concrete. The initial temperature of the concrete during casting is 25 °C, while the ambient temperature is maintained at 25 °C.
- (3) Data acquisition: The SH-16X multi-channel temperature data logger is used to collect data, starting from the moment the concrete is poured. The data

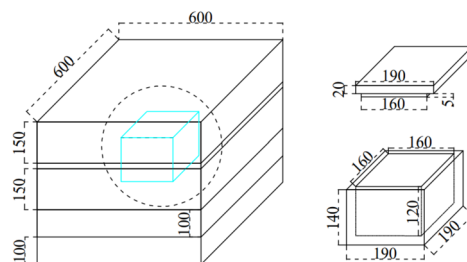


Fig. 5 Schematic diagram of semi-adiabatic box

logging frequency is set to record one data point per minute.

3 Result and Discussion

3.1 Analysis of Thermal Properties of BP

3.1.1 Analysis of Step Cooling Curve

Figure 6 illustrates the step cooling curve of BP, while Table 3 details the phase transition temperatures and durations for different phase change materials. During cooling, both 48#P and 5#P show a single phase transition plateau, with transition intervals of 48–49.9 °C and 4.6–5.8 °C, and durations of 33 min and 148 min, respectively. The step cooling curve of BP exhibits two plateau regions, representing the high-temperature and low-temperature phase transition stages. This indicates that the carbon atom composition of BP wax primarily concentrates within two specific ranges. During the high-temperature phase transition, the wax undergoes a

solid–liquid transition, while during the low-temperature phase transition, it undergoes a solid–solid transition.

As the mass fraction of 5#P increases, the high-temperature phase transition temperature and its duration gradually decrease, while the low-temperature phase transition temperature and duration increase. Compared to 48# paraffin, the high-temperature phase transition temperature and duration are both lower, occurring primarily between 18.3 and 47.3 °C. Similarly, the low-temperature phase transition temperature and duration are also lower than those of 5# wax, typically ranging between 0.1 and 4.6 °C. 5# paraffin is rich in low-chain hydrocarbon molecules, whereas 48# paraffin is abundant in high-chain hydrocarbon molecules. The interaction between high- and low-chain hydrocarbon molecules in the binary paraffin system results in its distinct phase transition behavior. This study focuses on H3 as the research subject for mass concrete applications in cold regions.

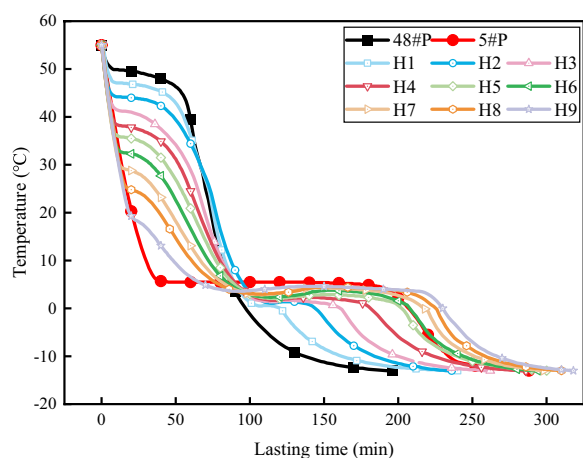


Fig. 6 Step cooling curve of BP

3.1.2 Analysis of Cold Storage and Discharge Curve

Figure 7 illustrates the cold storage and discharge curve of H3, detailing ten distinct stages. In the first stage (AB), the temperature of H3 drops rapidly. In the second stage (BC), the cooling rate slows significantly, forming a plateau region. At this point, the liquid paraffin begins to crystallize, gradually transitioning from a liquid to a gel state until it solidifies, releasing latent heat. In the third stage (CD), the temperature of H3 drops rapidly again. In the fourth stage (DE), as the temperature drops to approximately 1.5 °C, another plateau forms. Although there is no significant change in state, latent heat continues to be released. In the fifth stage (EF), the temperature continues to drop, but the rate gradually slows until it approaches ambient temperature, marking the end of the cooling process. In the sixth stage (FG), the temperature

Table 3 Phase transition temperature and phase transition duration of BP

Serial number	High-temperature phase transition range (°C)	Phase transition durations (min)	Low-temperature phase transition range (°C)	Phase transition durations (min)
48#P	48–49.9	33	–	–
5#P	–	–	4.6–5.8	148
H1	45.5–47.3	31	0.1–0.9	20
H2	43.0–44.3	27	1.0–1.4	28
H3	39.0–41.5	22	1.1–1.7	44
H4	37.1–38.4	18	1.8–2.3	60
H5	35.1–36.0	14	1.8–2.9	89
H6	32.0–32.7	11	2.8–3.3	92
H7	28.9–29.3	8	3.2–4.3	100
H8	24.4–25.0	6	3.4–4.5	112
H9	18.3–18.4	3	3.5–4.6	134

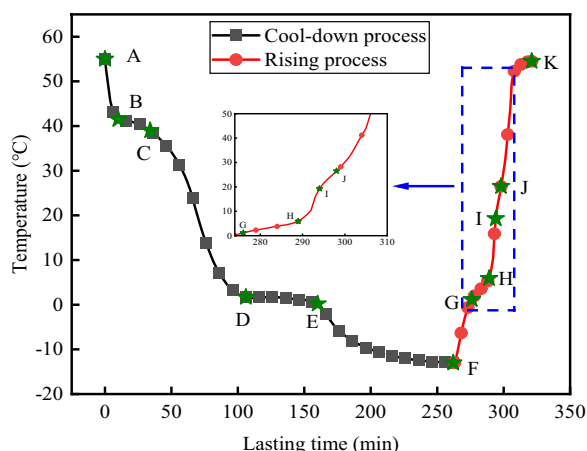


Fig. 7 The storage and release cold curve of H3

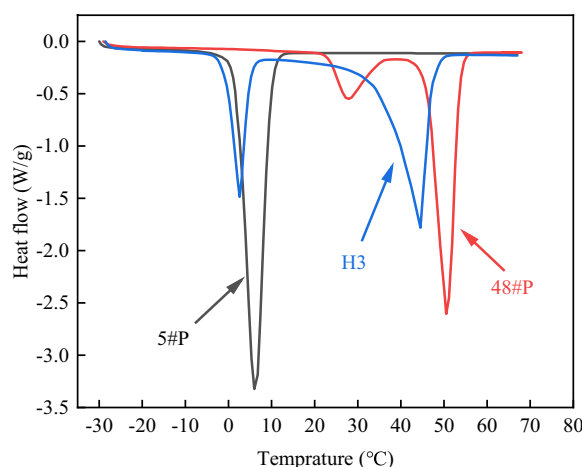


Fig. 8 DSC curves for 5#, 48#, and H3

quickly rises to around 2 °C. In the seventh stage (GH), the rate of temperature increase slows, indicating a gentle rise region with no significant change in state. In the eighth stage (HI), the rate of temperature increase accelerates again, and when the temperature reaches approximately 20 °C, H3 near the wall of the conical bottle gradually transitions from a solid to a liquid state. In the ninth stage (IJ), the rate of temperature increase slows again, though slightly faster than in the GH segment, during which H3 rapidly transitions from a solid to a liquid state. Finally, in the tenth stage (JK segment), H3 completely melts into a liquid, and the temperature continues to rise until it approaches that of the water bath.

The cold storage and discharge curve indicates that H3 demonstrates excellent phase change performance, with minimal evidence of supercooling. Phase change plateaus are observed during both heating and cooling processes, effectively delaying temperature fluctuations.

3.1.3 Analysis of DSC

Figure 8 shows the differential scanning calorimetry (DSC) curves for 48#P, 5#P, and H3, with the corresponding thermal parameters listed in Table 4. The DSC curve for 5#P shows a phase transition peak at 5.97 °C, with a corresponding phase change enthalpy of 200.84 J/g. The DSC curve for paraffin 48# displays two distinct endothermic peaks, with phase transition temperatures of 27.91 °C and 50.50 °C, and corresponding phase change enthalpies of 30.57 J/g and 136.78 J/g, respectively. The DSC curve of the H3 also shows two endothermic peaks at 2.58 °C and 44.52 °C, with corresponding enthalpies of 66.52 J/g and 102.63 J/g, respectively. The two endothermic peaks in paraffin 48# and the binary paraffin mixture indicate the presence of alkanes with varying carbon chain lengths.

Upon mixing, the temperatures and enthalpies of both absorption peaks of H3 shifted downward. The

Table 4 Thermal performance parameters of 5#, 48# and H3

PCMs	T ₀ (°C)	T _e (°C)	T _p (°C)	ΔH(J/g)
48#P	1.56	12.17	5.97	200.84
5#P	21.70	36.11	27.91	30.57
	41.59	56.18	50.50	136.78
H3	0.21	5.25	2.58	66.52
	34.17	49.92	44.52	102.63

T₀ is the initial melting temperature, T_e is the complete melting temperature, T_p is the Peak temperature of phase transition, and ΔH is the latent heat of phase change

high-temperature phase transition temperature and enthalpy decreased compared to pure paraffin 48#, while the low-temperature phase transition temperature and enthalpy decreased relative to pure paraffin 5#. Some low-chain alkane molecules in paraffin 5# interact with the high-chain alkane molecules in paraffin 48#, disrupting the crystalline structure of the high-chain alkanes. This interaction leads to a reduction in both the high-temperature phase transition temperature and enthalpy. The remaining low-chain alkane molecules form a more disordered molecular arrangement due to the mixing, making the structure easier to disrupt. This irregularity leads to a decrease in both the phase transition temperature and enthalpy (Zuo et al., 2023).

3.1.4 Analysis of Phase Transition Stability

The H3 step cooling curves after multiple phase transition cycles are shown in Fig. 9. After 50, 100, and 200 phase transition cycles, the initial temperatures of the high-temperature phase transition were 41.4 °C, 41.2 °C, and 40.6 °C, reflecting changes of 0.1 °C, 0.3 °C, and 0.9 °C, respectively. Similarly, the initial temperatures of

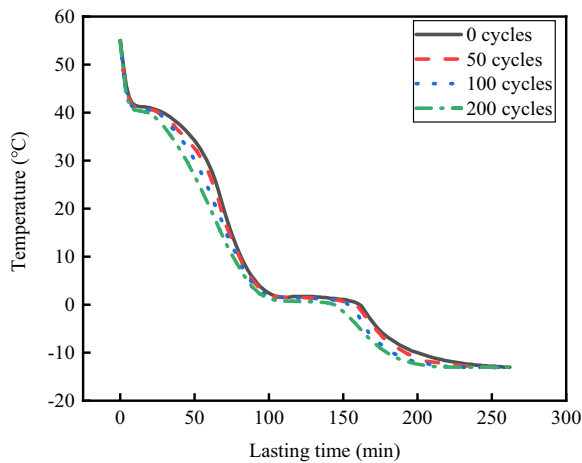


Fig. 9 Step cooling curves of H3 after several cycles

the low-temperature phase transition were 1.7 °C, 1.6 °C, and 1.4 °C, with corresponding changes of 0.1 °C, 0.2 °C, and 0.4 °C, respectively. These results suggest that H3 demonstrates excellent thermal cycle stability, with no significant decrease in phase transition temperature after multiple cycles.

3.2 Analysis of Phase Change Aggregate Packaging Effect

Figure 10 illustrates the mass change of phase change aggregates under continuous high-temperature conditions. The mass loss rates of EP_A after 12, 24, and 48 h of high-temperature exposure were 0.44%, 0.60%, and 0.68%, respectively. Under the same conditions, the mass loss rates of EP_{AD} were 0.30%, 0.40%, and 0.46%, while those of EP_{AW} were 0.24%, 0.32%, and 0.38%. Figure 11 illustrates the mass change of phase change aggregates after multiple phase change cycles. The graph clearly shows that as the number of phase

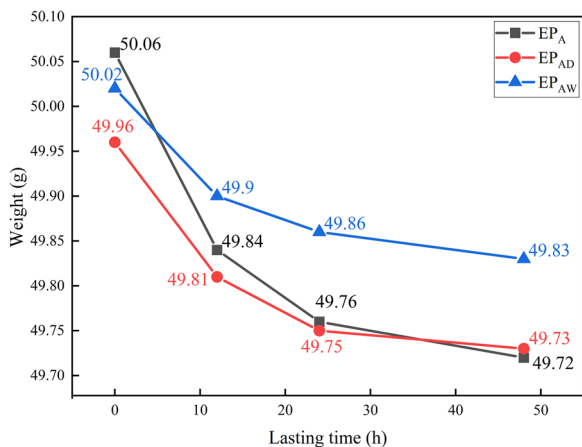


Fig. 10 The mass of phase change aggregates under continuous high-temperature conditions

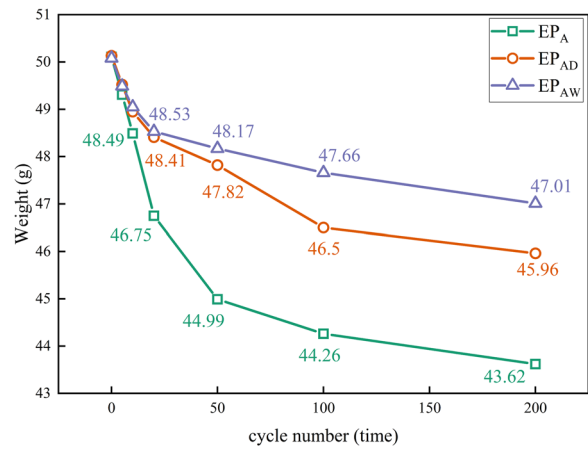


Fig. 11 The mass of phase change aggregates after multiple phase change cycles

change cycles increases, the mass of the phase change expanded perlite gradually decreases and eventually stabilizes. After 200 phase change cycles, the mass loss of EP_A reached 12.96%, while EP_{AD} experienced a mass loss of 8.32% and EP_{AW} only 6.14%. These results indicate that encapsulation effectively reduces the mass loss of PCMs and improves their stability during phase change cycles, with wet encapsulation proving the most effective.

3.3 Thermal Performance Analysis of Phase Change Concrete

3.3.1 Analysis of Thermal Conductivity

Figure 12 illustrates the relationship between the thermal conductivity of phase change concrete and the aggregate replacement rate. After 28 days of curing, it was observed

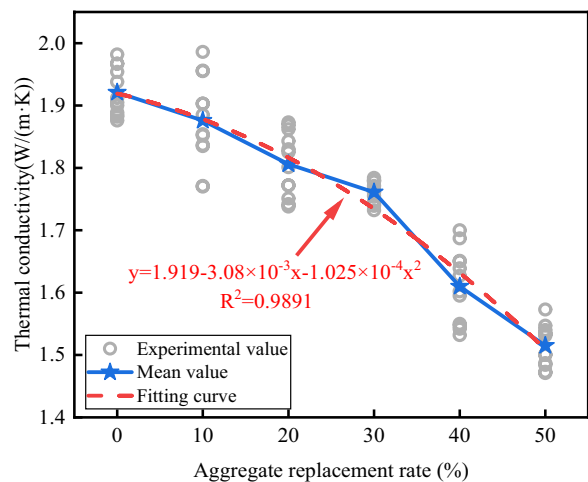


Fig. 12 Relationship between thermal conductivity and aggregate replacement rate

that as the aggregate replacement rate increases, the thermal conductivity of the concrete decreases significantly. Specifically, when the replacement rate increased from 10 to 50%, the thermal conductivity of the phase change concrete decreased by 2.34%, 5.99%, 8.33%, 16.19%, and 21.13%, respectively, compared to the reference concrete. Upon fitting these data, a nonlinear trend was identified between thermal conductivity and aggregate replacement rate, with the reduction in thermal conductivity gradually increasing as the replacement rate rises. Phase change aggregates have a porous and loose structure, leading to significantly lower thermal conductivity compared to river sand. Consequently, when phase change aggregates replace part of the river sand, the number of pores in the concrete increases, which in turn reduces the overall thermal conductivity (Guo et al., 2020). Moreover, phase change aggregates generally have larger particle sizes compared to river sand, which further impedes heat conduction and contributes to the reduction in thermal conductivity of phase change concrete (Zhang et al., 2015).

Figure 13 illustrates the trend in thermal conductivity of concrete at different ages. The thermal conductivity shows a non-linear decrease with age, with the rate of decrease gradually slowing down. As hydration progresses, the internal structure of concrete becomes denser, which typically increases thermal conductivity. Conversely, the hydration process also transforms clinker phase cementitious material into hydration products with lower thermal conductivity (Du & Ge, 2022). These opposing effects create a complex interplay that influences the thermal conductivity of concrete. Ultimately, the final thermal conductivity exhibits a decreasing trend, suggesting that the transformation into hydration products has a more pronounced effect on reducing thermal

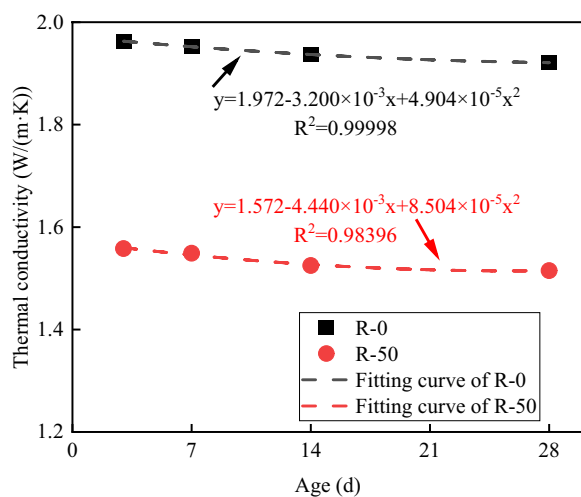


Fig. 13 Relationship between thermal conductivity and age

conductivity. Furthermore, the gradual attenuation of the hydration reaction over time mitigates the reduction in concrete’s thermal conductivity.

3.3.2 Analysis of Semi-adiabatic Temperature Rise

Figure 14 presents the temperature rise curve of phase change concrete under semi-adiabatic conditions, while Fig. 15 illustrates the evolution of its temperature rise rate. After pouring, phase change concrete exhibits a typical ‘S’-shaped temperature rise characteristic, similar to that of ordinary concrete, under semi-adiabatic conditions. Using ordinary concrete as an example, the adiabatic temperature rise process can be divided into three distinct stages.

- (1) The first stage is characterized by a slow temperature increase during the initial hydration period (0h–6.7h). During this phase, the hydration reaction within the concrete is not fully developed, leading to a slow temperature rise, with the rate of increase remaining low, between 0 and 0.2°C/h.
- (2) The second stage is marked by a rapid temperature rise during the mid-hydration period (6.7h–24.5h). Heat accumulates quickly within the concrete, causing a sharp increase in temperature. During this phase, the rate of temperature rise accelerates significantly, reaching 0.2 to 3.1 °C/h.
- (3) The third stage is characterized by stabilization during the late hydration period (24.5–32 h). As the hydration reaction nears completion, heat release within the concrete stabilizes, causing a marked slowdown in temperature rise, with the rate of increase gradually decreasing to 0.3 to 0 °C/h.

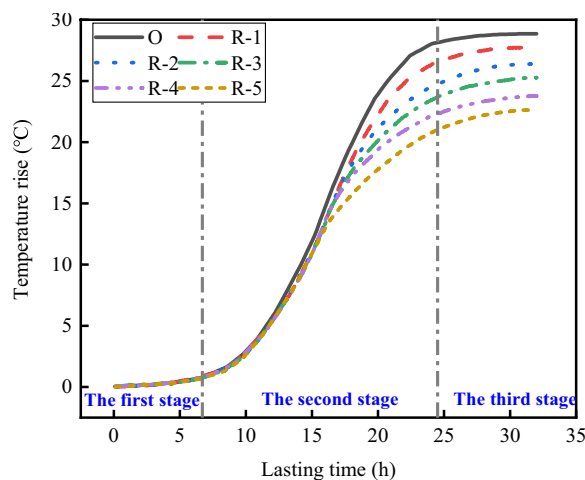


Fig. 14 Semi-adiabatic temperature rise curve of phase change concrete

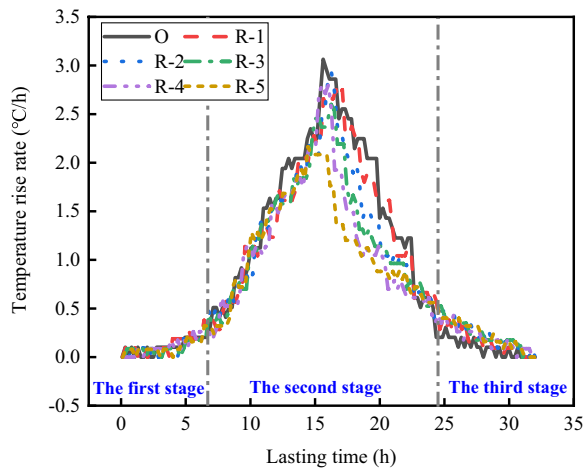


Fig. 15 Semi-adiabatic temperature rise rate of phase change concrete

The experimental results indicate that after 24 h under semi-adiabatic conditions, the temperature rise values of phase change concretes R-1 to R-5 decreased by 4.50%, 9.34%, 12.46%, 19.03%, and 21.80%, respectively, compared to the reference concrete R-0. As the replacement rate of phase change aggregate increases, the peak temperature rise rate of concrete gradually decreases, and the duration of high temperature rise rates (greater than 1.5 °C/h) shortens accordingly. This suggests that adding phase change aggregate effectively mitigates sharp temperature fluctuations in concrete, thereby improving its thermal performance.

4 Semi-adiabatic Temperature Rise Model of Concrete

4.1 Ordinary Concrete

Three models, namely exponential, hyperbolic, and composite exponential models (Zhu, 1999), were employed to fit and investigate the semi-adiabatic temperature rise process of ordinary concrete, as shown in Fig. 16. Table 5 lists the parameter values of each fitting model. Through comparison, it was observed that there were significant deviations between the exponential and hyperbolic fitting curves and the measured data, indicating unsatisfactory fitting performance. Conversely, the composite exponential model exhibited a high fitting degree of 0.9998, demonstrating extremely high fitting accuracy, with its fitting curve highly consistent with the measured data. Therefore, the composite exponential model can accurately describe the early-stage adiabatic temperature rise process of ordinary concrete.

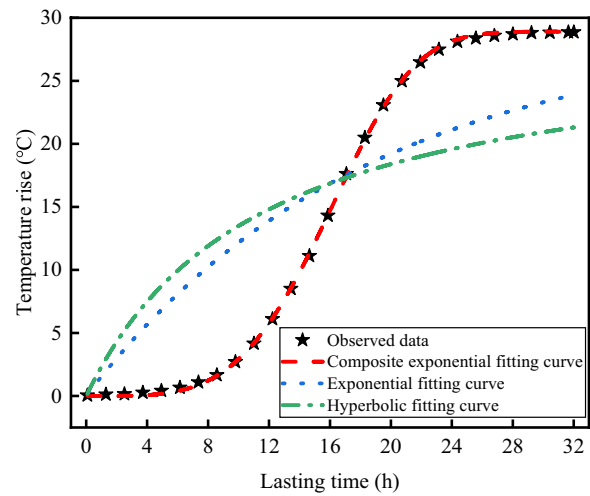


Fig. 16 Fitting curve of semi-adiabatic temperature rise model for Ordinary concrete

Table 5 Fitting parameters of semi-adiabatic temperature rise model

Model	θ_0 /°C	Expression	R ²
Exponential	28.9	$\theta(t) = 28.9(1 - e^{-0.055t})$	0.7367
Hyperbolic	28.9	$\theta(t) = \frac{28.9t}{11.417+t}$	0.9410
Composite exponential	28.9	$\theta(t) = 28.9(1 - e^{-1.002 \times 10^{-5} t^{4.028}})$	0.9998

θ_0 is the adiabatic temperature rise

4.2 Phase Change Concrete

The temperature rise process of phase change concrete under semi-adiabatic conditions exhibits similar developmental patterns to ordinary concrete, providing a basis for fitting using the composite exponential model. Figure 17 depicts the fitting curve, with the model parameters listed in Table 8. It can be observed that the fitting results are highly consistent with the measured data, with R² values exceeding 0.99. The utilization of the composite exponential model effectively reflects the exothermic process of hydration in phase change concrete (Table 6).

4.3 Analysis of Parameter

4.3.1 θ_0

During the semi-adiabatic temperature rise of concrete, energy conservation is upheld, whereby the change in internal energy is equal to the sum of the inflow (or out-flow) heat and the heat generated by the internal heat source, as depicted in Eq. (1).

$$\rho c \theta_0 = (1 - \varphi) m Q_0 - \alpha \beta \Delta H \tag{1}$$

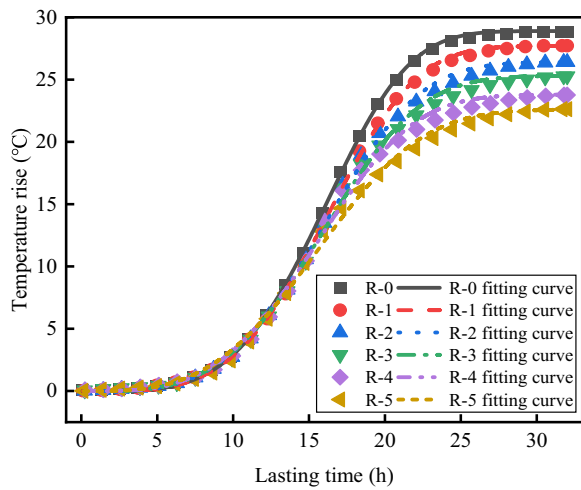


Fig. 17 Fitting curve of semi-adiabatic temperature rise model for phase change concrete

Table 6 Parameters of semi-adiabatic temperature rise model

Serial number	$\theta_0/^\circ\text{C}$	$a/10^{-5}$	b	R^2
R-0	28.9	1.002	4.028	0.9998
R-1	27.6	1.394	3.891	0.9997
R-2	26.2	2.962	3.633	0.9988
R-3	25.3	3.707	3.560	0.9984
R-4	23.4	4.437	3.521	0.9977
R-5	22.6	8.379	3.286	0.9977

Table 7 The specific heat capacity value of concrete

Serial number	R-0	R-1	R-2	R-3	R-4	R-5
c ($\text{kJ kg}^{-1} \text{ }^\circ\text{C}^{-1}$)	0.97	1.01	1.06	1.11	1.18	1.23

Table 8 Comparison between calculated value and experimental value of θ_0

Serial number	R-0	R-1	R-2	R-3	R-4	R-5
Calculated value ($^\circ\text{C}$)	28.8	27.7	26.4	25.3	23.8	22.9
Experimental value ($^\circ\text{C}$)	28.9	27.6	26.2	25.3	23.4	22.6
Absolute error ($^\circ\text{C}$)	-0.1	0.1	0.2	0	0.4	0.3
RMSE	0.2273					
MAPE (%)	4.5085					

where ρ represents the density of phase change concrete (kg/m^3), c represents the specific heat of phase change concrete [$\text{kJ}/(\text{kg } ^\circ\text{C})$], as shown in Table 7, ϕ represents the heat loss rate, and the value is 10–12%, m represents the mass of cementitious material per cubic meter of concrete; Q_0 indicates the early cumulative hydration heat of cementitious materials (kJ/kg), and the value is 138.3–141.4 kJ/kg , α denotes the mass of phase change aggregate per cubic meter of concrete in kilograms per cubic meter (kg/m^3); and β represents the proportion of phase change paraffin in the phase change aggregate.

Based on the calculation results obtained from formula (1), the adiabatic temperature rise of phase change concrete is summarized in Table 8. The absolute error of the semi-adiabatic temperature rise is rigorously constrained to within 0.4°C . Moreover, the root mean square error is less than 0.5, and the average absolute percentage error is below 10%. These findings unequivocally demonstrate that Eq. (1) exhibits a high level of accuracy in predicting the semi-adiabatic temperature rise of phase change concrete.

4.3.2 Parameters a and b

Figure 18 illustrate the relationships between model parameters and the aggregate replacement rate. Through fitting analysis, it can be observed that as the aggregate replacement rate increases, parameter a exhibits a nonlinear increase, while parameter b shows a linear decrease.

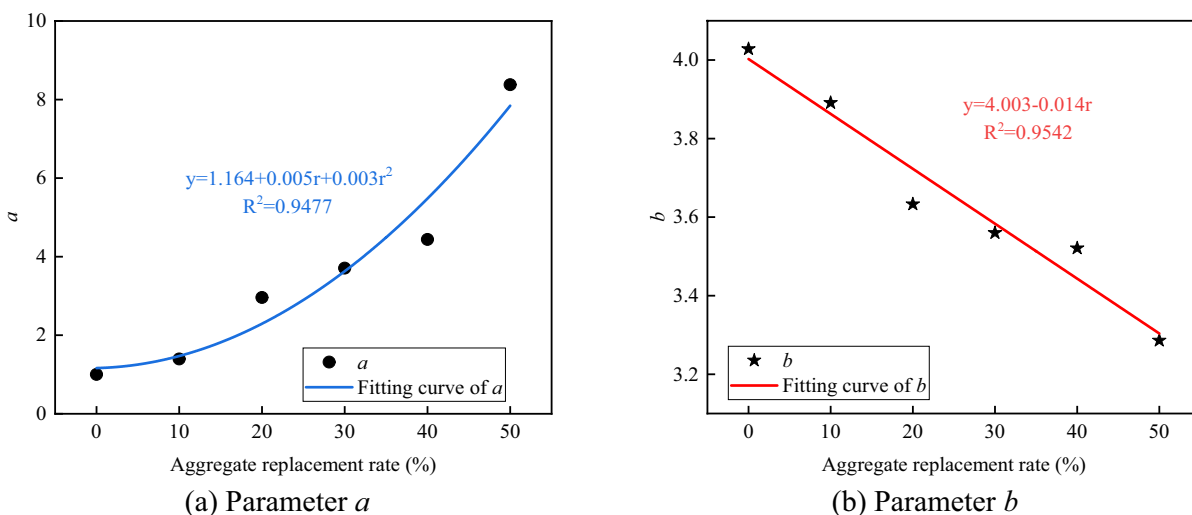


Fig. 18 The relationship of the parameters to the replacement rate

5 Conclusions

BP was developed using the melt blending method, and its thermal properties were thoroughly evaluated. Expanded perlite served as the carrier material, while cement paste was employed as the encapsulating medium to produce phase change fine aggregates. Phase change concrete was prepared by replacing sand using the equal volume replacement method, and its semi-adiabatic temperature rise and thermal conductivity were analyzed. The following conclusions were drawn:

- (1) During the cooling process of BP, two distinct phase transition temperatures were observed. As the mass fraction of 5#P increased, the high-temperature phase transition temperature and its corresponding duration decreased significantly, while the low-temperature phase transition temperature and duration increased. Notably, the H3 material exhibited two prominent endothermic peaks, with phase transition temperatures of 2.58°C and 44.52°C, and corresponding latent heats of 66.52 J/g and 102.63 J/g, respectively. Additionally, the step cooling curve of H3 could be divided into ten stages. Even after multiple cycles, it demonstrated excellent phase change performance.
- (2) The incorporation of phase change aggregate reduces the thermal conductivity of concrete, with the thermal conductivity coefficient decreasing in a parabolic pattern as the aggregate replacement rate increases. The thermal conductivity of concrete decreases over time. In the early stage (3–14 days), phase change concrete exhibits a more significant

reduction in thermal conductivity compared to ordinary concrete. However, in the later stage (14–28 days), this reduction becomes smaller than that observed in ordinary concrete.

- (3) The inclusion of phase change aggregate significantly reduces the hydration temperature rise in concrete and effectively slows the rate of temperature increase. As the replacement rate of phase change aggregate increases, the temperature rise consistently decreases. The semi-adiabatic temperature rise curve shows a characteristic “S”-shaped variation over time, which can be clearly divided into three stages: an initial slow heating stage (0 h–6.7 h), followed by a rapid heating stage (6.7 h–24.5 h), and finally, a stable stage (24.5 h–32 h). The study concluded that the composite exponential model accurately reflects the semi-adiabatic temperature rise process in phase change concrete.

Acknowledgements

Thank you very much for the experimental guidance given by the teachers and brothers of the research group in the course of this study, for the guidance of Professor Li Dongwei in the experimental scheme, for the technical guidance of Chen Tao’s brother in the use of instruments, and for the help given by Zhongshiming’s brother in the sample preparation process. The authors would like to thank the reviewers for their valuable suggestions and comments to improve the quality of the paper.

Author contributions

Jia Zhiwen wrote the main manuscript text and designed the experiments. Wang Zecheng and Fang Fang conducted the tests. Li Dongwei and Wang Zhenhua reviewed and edited the draft. Li Dongwei and Wang Zhenhua provided funding support.

Funding

The financial support of the National Natural Science Foundation of China (No. 42061011 and 41977236) and the Key Research and Development Programs of Jiangxi Province (NO. 20232BBE50025 and 20223BBG71W01).

Data availability

All data generated or analysed during this study are included in this published article.

Declarations

Competing interests

The authors declare that they have no competing interests.

Received: 26 May 2024 Accepted: 17 September 2024

Published online: 05 December 2024

References

- Afzal, J., Yihong, Z., Aslam, M., & Qayum, M. (2022). A study on thermal analysis of under-construction concrete dam. *Case Studies in Construction Materials*, 17, e01206. <https://doi.org/10.1016/j.cscm.2022.e01206>
- Bai, J., Yuan, Z., Liu, Y., Zhang, Y., & Lv, X. (2022). Fabrication and thermal properties of decanoic acid-paraffin/graphene aerogel form-stable phase change materials. *Chemical Industry and Engineering Progress*, 41(8), 4441–4448. <https://doi.org/10.16085/j.issn.1000-6613.2021-2102>
- Berardi, U., & Gallardo, A. A. (2019). Properties of concretes enhanced with phase change materials for building applications. *Energy and Buildings*, 199, 402–414. <https://doi.org/10.1016/j.enbuild.2019.07.014>
- Chen, C., Ma, F., & Wang, Y. (2022). Effect of shape stabilized binary paraffin on properties of desulfurization gypsum-based composites. *Journal of Building Materials*, 25(7), 708–714.
- Dong, M., Li, S., Yu, B., Jiang, Q., Zhu, H., Zhao, J., Huang, J., & Tao, S. (2024). Experimental investigation on the freeze-thaw durability of a phase change concrete in cold regions. *Cold Regions Science and Technology*, 218, 104102. <https://doi.org/10.1016/j.coldregions.2023.104102>
- Du, Y., & Ge, Y. (2022). Modeling of effective thermal conductivity of cement paste. *Journal of the Chinese Ceramic Society*, 50(2), 466–472. <https://doi.org/10.14062/j.issn.0454-5648.20210431>
- Fernandes, F., Manari, S., Aguayo, M., Santos, K., Oey, T., Wei, Z., Falzone, G., Neithalath, N., & Sant, G. (2014). On the feasibility of using phase change materials (PCMs) to mitigate thermal cracking in cementitious materials. *Cement & Concrete Composites*, 51, 14–26. <https://doi.org/10.1016/j.cemconcomp.2014.03.003>
- Ghadim, H. B., Shahbaz, K., Al-Shannaq, R., & Farid, M. M. (2019). Binary mixtures of fatty alcohols and fatty acid esters as novel solid-liquid phase change materials. *International Journal of Energy Research*, 43(14), 8536–8547. <https://doi.org/10.1002/er.4852>
- Guo, P., Bu, M., Li, Q., & He, M. (2020). Research progress of accurate measurement and characterization model of effective thermal conductivity of rock. *Chinese Journal of Rock Mechanics and Engineering*, 39(10), 1983–2013. <https://doi.org/10.13722/j.cnki.jrme.2020.0337>
- Hamid, H., & Chorzepe, M. G. (2020). Quantifying maximum temperature in 17 mass concrete cube specimens made with mixtures including metakaolin and/or slag. *Construction and Building Materials*, 252, 118950. <https://doi.org/10.1016/j.conbuildmat.2020.118950>
- Ju, S., Wang, F., Zhang, J., Shi, J., Jiang, J., Wang, L., & Liu, Z. (2023). A robust, compatible, and effective core-shell structured phase change materials for controlling the temperature rise caused by cement hydration. *Journal of Building Engineering*, 80, 107906. <https://doi.org/10.1016/j.jobe.2023.107906>
- Kheradmand, M., Vicente, R., Azenha, M., & de Aguiar, J. L. B. (2019). Influence of the incorporation of phase change materials on temperature development in mortar at early ages: Experiments and numerical simulation. *Construction and Building Materials*, 225, 1036–1051. <https://doi.org/10.1016/j.conbuildmat.2019.08.028>
- Kim, Y.-R., Khil, B.-S., Jang, S.-J., Choi, W.-C., & Yun, H.-D. (2015). Effect of barium-based phase change material (PCM) to control the heat of hydration on the mechanical properties of mass concrete. *Thermochimica Acta*, 613, 100–107. <https://doi.org/10.1016/j.tca.2015.05.025>
- Li, D., Jia, Z., Wang, Z., Xue, K., Wang, Z., & Fang, F. (2024). Experimental and numerical study on the model of hybrid fiber phase change concrete frozen shaft wall. *PLoS ONE*, 19(8), e0306984.
- Li, L., Chen, M., Guo, X., Lu, L., Wang, S., Cheng, X., & Wang, K. (2020). Early-age hydration characteristics and kinetics of Portland cement pastes with super low w/c ratios using ice particles as mixing water. *Journal of Materials Research and Technology*, 9(4), 8407–8428. <https://doi.org/10.1016/j.jmrt.2020.05.082>
- Li, L., Dabarera, A., & Vinh, D. (2022). Evaluation of zero-stress temperature and cracking temperature of high performance concrete at early ages. *Materials and Structures*, 55(7), 181. <https://doi.org/10.1617/s11527-022-02019-2>
- Li, X., Yu, Z., Chen, K., Deng, C., & Yu, F. (2023). Investigation of temperature development and cracking control strategies of mass concrete: A field monitoring case study. *Case Studies in Construction Materials*, 18, e02144. <https://doi.org/10.1016/j.cscm.2023.e02144>
- Lu, X., Chen, B., Tian, B., Li, Y., Lv, C., & Xiong, B. (2021). A new method for hydraulic mass concrete temperature control: Design and experiment. *Construction and Building Materials*, 302, 124167. <https://doi.org/10.1016/j.conbuildmat.2021.124167>
- Luo, T., Wang, X., & Zhuang, S. (2023). Value-added utilization of steel slag as a hydration heat controlling material to prepare sustainable and green mass concrete. *Case Studies in Construction Materials*, 19, e02619. <https://doi.org/10.1016/j.cscm.2023.e02619>
- Lv, Y., Jin, W., Yang, Y., Zhang, H., Zhang, X., Ding, F., & Zhou, W. (2017). Experimental thermal storage research of organic binary phase change materials in building environment. *International Journal of Green Energy*, 14(11), 916–924. <https://doi.org/10.1080/15435075.2017.1339042>
- Mandal, S., Ishak, S., Singh, J. K., Lee, D.-E., & Park, T. (2022). Synthesis and application of paraffin/silica phase change nanocapsules: Experimental and numerical approach. *Journal of Energy Storage*, 51, 104407. <https://doi.org/10.1016/j.est.2022.104407>
- Mardmomen, S., & Chen, H.-L. (2023). Prediction of the early age thermal behavior of mass concrete containing SCMs using Ansys. *Journal of Thermal Analysis and Calorimetry*, 148(15), 7899–7917. <https://doi.org/10.1007/s10973-023-12243-9>
- Savija, B., & Schlangen, E. (2016). Use of phase change materials (PCMs) to mitigate early age thermal cracking in concrete: Theoretical considerations. *Construction and Building Materials*, 126, 332–344. <https://doi.org/10.1016/j.conbuildmat.2016.09.046>
- Shen, Y., Lv, Y., Yang, H., Ma, W., Zhang, L., & Pan, J. (2022). Effect of different ice contents on heat transfer and mechanical properties of concrete. *Cold Regions Science and Technology*, 199, 103570. <https://doi.org/10.1016/j.coldregions.2022.103570>
- Shu, Z., Zhong, K., Xiao, X., Jia, H., Lv, F., & Chang, S. (2021). Recent progress in application of composite phase change materials with nanoparticles matrix for energy savings of buildings. *Chemical Industry and Engineering Progress*, 40(S2), 265–278. <https://doi.org/10.16085/j.issn.1000-6613.2021-0482>
- Singh, M. P., Sen, S., Pathak, H., & Dogra, A. B. (2024). Early age cracking relevant to mass concrete dam structures during the construction schedule. *Construction and Building Materials*, 411, 134739. <https://doi.org/10.1016/j.conbuildmat.2023.134739>
- Smolana, A., Klemczak, B., Azenha, M., & Schlicke, D. (2021). Early age cracking risk in a massive concrete foundation slab: Comparison of analytical and numerical prediction models with on-site measurements. *Construction and Building Materials*, 301, 124135. <https://doi.org/10.1016/j.conbuildmat.2021.124135>
- Tasri, A., & Susilawati, A. (2019). Effect of material of post-cooling pipes on temperature and thermal stress in mass concrete. *Structures*, 20, 204–212. <https://doi.org/10.1016/j.istruc.2019.03.015>
- Tian, Y., Lai, Y., Qin, Z., & Pei, W. (2022). Numerical investigation on the thermal control performance and freeze-thaw resistance of a composite concrete pier with microencapsulated phase change materials. *Solar Energy*, 231, 970–984. <https://doi.org/10.1016/j.solener.2021.12.042>
- Tran, M. V., Chau, V. N., & Nguyen, P. H. (2023). Prediction and control of temperature rise of massive reinforced concrete transfer slab with embedded cooling pipe. *Case Studies in Construction Materials*, 18, e01817. <https://doi.org/10.1016/j.cscm.2022.e01817>

- Wang, J., Wei, G., Liu, J., Chen, J., & Zuo, Y. (2020). Measurement and analysis of hydration heat in massive concrete pile cap of a sea-crossing bridge. *Bridge Construction*, 50(3), 25–31.
- Wang, Q., Liu, R., Liu, C., Liu, P., & Sun, L. (2022). Effects of silica fume type and cementitious material content on the adiabatic temperature rise behavior of LHP cement concrete. *Construction and Building Materials*, 351, 128976. <https://doi.org/10.1016/j.conbuildmat.2022.128976>
- Wang, Y.-S., Mo, L.-H., Xie, S.-X., Wang, C.-Y., Yu, X.-B., & Zhou, H. (2023). Early-age cracking in mass concrete: Modeling and case study of an extra-large exhibition pool. *Journal of Building Engineering*, 80, 108118. <https://doi.org/10.1016/j.jobe.2023.108118>
- Wang, Z., Zhang, W., Wang, R., Deng, W., & Wu, Y. (2022). Influence of paraffin thermal media on adiabatic temperature rise of concrete. *Materials Reports*, 36(S1), 314–318.
- Xie, Y., Du, W., Xu, Y., Peng, B., & Qian, C. (2023). Temperature field evolution of mass concrete: From hydration dynamics, finite element models to real concrete structure. *Journal of Building Engineering*, 65, 105699. <https://doi.org/10.1016/j.jobe.2022.105699>
- Yun, H.-D., Ahn, K.-L., Jang, S.-J., Khil, B.-S., Park, W.-S., & Kim, S.-W. (2019). Thermal and mechanical behaviors of concrete with incorporation of strontium-based phase change material (PCM). *International Journal of Concrete Structures and Materials*, 13(1), 18. <https://doi.org/10.1186/s40069-018-0326-8>
- Zhang, J., Li, F., Liu, S., Wu, W., & Yu, X. (2022). Early age cracking potential of inner lining of coal mine frozen shaft. *Energy Reports Presented at the International Conference on New Energy and Power Engineering (ICNEPE)*, 8, 16–24. <https://doi.org/10.1016/j.egy.2022.01.132>
- Zhang, T., Yang, W., Chen, G., Huang, J., Han, T., & Zhang, C. (2016). Monitoring and analysis of hydration heat temperature field for high performance mass concrete freezing shaft lining. *Journal of Mining & Safety Engineering*, 33(2), 290–296. <https://doi.org/10.13545/j.cnki.jmse.2016.02.016>
- Zhang, W., Tong, F., Xing, Y., & Gu, X. (2015). Experimental study and prediction model of thermal conductivity of concrete. *Journal of Building Materials*, 18(2), 183–189.
- Zhang, Y. (2023). Thermal cracking in high volume of fly ash and GGBFS concrete. *International Journal of Concrete Structures and Materials*, 17(1), 65. <https://doi.org/10.1186/s40069-023-00626-z>
- Zhang, Y., Wang, S., He, S., & Hao, X. (2023). Analysis of factors influencing the temperature field variation in mass concrete during hydration heat release. *Case Studies in Thermal Engineering*, 52, 103737. <https://doi.org/10.1016/j.csite.2023.103737>
- Zhao, Z., Wang, K., Lange, D. A., Zhou, H., Wang, W., & Zhu, D. (2019). Creep and thermal cracking of ultra-high volume fly ash mass concrete at early age. *Cement & Concrete Composites*, 99, 191–202. <https://doi.org/10.1016/j.cemconcomp.2019.02.018>
- Zhou, X., Guan, H., & Zhang, L. (2017). Temperature field research of mass concrete based on the phase change condition of ground freezing wall. *Journal of Basic Science and Engineering*, 25(2), 395–406. <https://doi.org/10.16058/j.issn.1005-0930.2017.02.017>
- Zhu, B. F. (1999). *Temperature stress and temperature control of mass concrete*. China Electric Power Press.
- Zuo, P., Liu, Z., Zhang, H., Dai, D., Fu, Z., Corker, J., & Fan, M. (2023). Formulation and phase change mechanism of Capric acid/Octadecanol binary composite phase change materials. *Energy*, 270, 126943. <https://doi.org/10.1016/j.energy.2023.126943>

Publisher's Note

Springer Nature remains neutral with regard to jurisdictional claims in published maps and institutional affiliations.

Zhiwen Jia Doctoral student, School of Civil and Architectural Engineering, East China University of Technology, Nanchang 330013, China.

Dongwei Li Professor, College of Civil Engineering and Architecture, Dalian University, Dalian 116622, China.

Zecheng Wang Doctoral student, School of Civil and Architectural Engineering, East China University of Technology, Nanchang 330013, China.

Zhenhua Wang Associate Professor, School of Civil and Architectural Engineering, East China University of Technology, Nanchang 330013, China.

Fang Fang Postgraduates, School of Civil and Architectural Engineering, East China University of Technology, Nanchang 330013, China.